46th AIAA/ASME/ASCE/AHS/ASC Structures, Structural Dynamics & Materials Conference
18 - 21 April 2005, Austin, Texas

AIAA 2005-2320

AIAA 2005-2320

Discrete Cohesive Zone Model To Simulate Static Fracture In Carbon Fiber Textile Composites

De Xie[♣], *Amit G. Salvi*[♠], *Anthony M. Waas*[♦] *and Ari Caliskan*[*]

A discrete cohesive zone model (DCZM) is developed to simulate the mode I and mixed mode fracture. For the mode I case, experimental results generated using a modified single edge notched bend specimen of a 2D triaxially braided composite (2DTBC) are used to verify the DCZM. The 2DTBC is modeled as an elastic one-parameter ("a_{66}") plastic continuum. The plastic behavior of the 2DTBC is characterized by measuring a_{66}. Fracture toughness (G_{IC}) as a function of crack extension is measured by a compliance approach in the SENB tests. A previously developed mixed mode bending (MMB) fracture test configuration is a useful method to generate fracture envelopes for delamination failure of composites. The DCZM is used to simulate mixed mode fracture of a unidirectional laminated composite loaded using the MMB. The simulated results are compared with selected experimental results and also verified for mesh sensitivity. It is shown that the present DCZM is a versatile tool to study failure of a wide class of composite materials.

Introduction

Several industrial sectors are currently exploring ways to utilize a variety of different composite architectures for structural applications. These include continuous fiber pre-preg based laminated composites, woven and braided textile composites, sandwich composites, chopped fiber composites and low cost pultruded composites. Thus a need arises to develop a comprehensive understanding of the mechanical response and subsequent fracture of these different composite materials [1-15]. While the former is governed by an accurate knowledge of structural stiffness, the latter falls into the category of structural integrity. Classical linear elastic fracture mechanics (LEFM) based approaches and their extensions to account for material nonlinearity are the most commonly used tools in a structural integrity and damage tolerance analysis (SIDT). In SIDT, a structure with a flaw in the form of a crack is studied. The strain energy release rate is computed by the virtual crack closure technique (VCCT) and compared to

♣ Post Doctoral Student, University of Michigan, Ann Arbor, MI 48109.
♠ Graduate Student, University of Michigan, Ann Arbor, MI 48109.
♦ Professor, University of Michigan, Ann Arbor, MI 48109. Associate Fellow, AIAA. Corresponding author.
* Technical Expert, Vehicle Design Research & Advanced Engineering, Ford Motor Company, Dearborn, MI 48121.

an appropriate critical value measured from tests [16-20]. With a "go no-go" type criterion, crack growth is predicted. This is a computationally efficient approach for linear elastic materials. However, for a wide class of fiber composites, significant material nonlinear effects are observed at fracture initiation and subsequent growth [21, 22]. These nonlinearities may arise from matrix micro-cracking, matrix plasticity, fiber/matrix interface decohesion, and fiber bridging. An expedient way to deal with the effect of these nonlinearities is via a cohesive zone formulation [23].

Cohesive zone modeling has been extensively used in conjunction with continuum interface elements in finite element analysis (FEA) [24-43]. A historical account of the developments in cohesive zone modeling is presented in [44-45]. The interface cohesive elements, which are placed between the two surfaces that need to be decohered, are of zero thickness (initial zero separation between the surfaces). Depending on the formulation, the stiffness matrix of these interface elements may contain off-diagonal terms. In [46], a comprehensive overview of the different interface elements and their finite element formulation is provided. In particular, it is noted that smeared continuum cohesive elements (CCZM) lead to a fully populated stiffness matrix (equation 19 of [46]) while a discrete cohesive zone model (DCZM) leads to a very sparse interface element stiffness matrix (equation 27 of [46]). The main implication of this is the attendant computational time and robustness in the resulting computations. For instance, if the initial stiffness of the interface elements in the pre-cracking phase is chosen to be very large, then, as pointed out in [45], depending on the spatial integration scheme used, the CCZM shows spurious oscillations in the tractions. These oscillations are not an issue in DCZM, since the DCZM embodies, in spirit, the idea of point-wise separation, as advanced in [23, 47]. A major reason for both computational expediency and suppression of spurious oscillations can be attributed to the fact that CCZM uses interpolated displacements for embedment in the traction separation law, while essentially in the 1D DCZM models, the direct nodal displacement values are used in the traction separation laws.

The central idea of the present DCZM is to treat the cohesive zone as a discrete bed of 1D spring type elements [47-51]. A nonlinear discrete 1D element is placed between interfacial node pairs to model cohesive interactions between surfaces instead of using continuum elements along the crack path. In the present work, the DCZM adopted has three major differences compared to that discussed in [47-51]. First, in [47-51], the crack tip strain field (the characteristic $r^{-1/2}$ singularity) is incorporated in the construction of the spring models. This adds additional computational complication. Second, the DCZM presented here, is *scalable* according to the node spacing (i.e. mesh size) as will be shown subsequently. Indeed, there is precedent to such an idea as is presented in [52], in which the softening modulus is made a function of the element size. Finally, the present DCZM algorithm is amenable to problems where substantial rotations of the crack path can occur. In these instances, both geometric non-linearity and the local orientation of the crack path to account for the proper local mode mixity, as has been discussed in [38], need to be properly accounted for.

In this paper, the DCZM is used to simulate static mode I fracture of a 2DTBC and the mixed-mode fracture of a unidirectional fiber composite. The 2DTBC is treated as an elastic plastic orthotropic homogenized material. The effective mechanical properties (E_{11}, E_{22}, ν_{12} and G_{12}) are measured by using ASTM (American Society for Testing and Materials) specified standard material property tests. The plastic behavior of the material is characterized by carrying out static off-axis compression tests, from which the plasticity parameter “a_{66}” is obtained.

Mode I fracture tests are carried out to measure the fracture toughness (G_{IC}) as a function of crack growth. A compliance approach is used and it is found that the fracture toughness (G_{IC}) varies as the crack propagates in the specimen [22]. These variations are incorporated in the simulations using the DCZM based interface elements; through a UEL (user element option) within the commercial FEA software code ABAQUS. The simulated results agree very well with test data and are not sensitive to the FEA mesh density. This is quite attractive from a design/test/validation viewpoint and provides confidence in the use of DCZM for design applications.

Interface Element based on DCZM

Figure 1 shows the schemes for DCZM and CCZM. CCZM uses conventional continuum type elements while DCZM uses nonlinear two-noded axial elements. In related early work, these elements are referred to as spring elements (see, [23, 48-49]) however, incorporating details of the crack tip strain fields. As discussed earlier the present DCZM incorporates the nodal displacements across the decohesion surfaces directly into the traction separation law, which in turn is scalable with respect to the mesh size. The DCZM can be conveniently adopted into commercial software codes, for instance, by directly using the nonlinear spring element option provided by the ABAQUS® [51]. However, this must be handled with care particularly for problems that have significant nonlinearity (geometric or different loading and unloading paths) or for situations that present non-uniform fracture toughness. If the cohesive law varies along the crack path, as in the present study, or a non-uniform mesh is used, the data preparation could be cumbersome since the F-δ relation at each node pair should be defined individually. This makes automation difficult. If the cohesive law has a complicated form rather than a simple triangular shape, the data preparation for the F-δ relation could also be tedious.

In the present study, a discrete, two-noded interface element is introduced via a user subroutine UEL in ABAQUS® [53] in order to develop a universal DCZM in a generalized manner for simulating fracture. Figure 2 shows the element definition and node numbering adopted. The element is placed in such a way that the nodes 1 and 2 are located at the crack tip. Initially, node 1 coincides with node 2 and the gap between the two nodes, exaggerated in Figure 3, vanishes. Since the element has four nodes, the default instant displacement array for the element is {U_1, U_2, U_3, U_4, U_5, U_6, U_7 and U_8}, which includes "dummy" nodes.

In order to apply cohesive law at the crack tip, a DCZM element is placed between nodes "1" and "2". Nodes "3" and "4" are dummy nodes and do not have contributions to the stiffness matrix. They are introduced to extract information for finite crack orientation angle (θ) and the effective length (Δa). This is particularly important for problems that have significant geometric nonlinearity. Using Figure 2, it follows that,

$$\cos\theta = \frac{x_4 - x_1}{\sqrt{(x_4 - x_1)^2 + (y_4 - y_1)^2}} \quad \text{.....(1a)}$$

$$\sin\theta = \frac{y_4 - y_1}{\sqrt{(x_4 - x_1)^2 + (y_4 - y_1)^2}} \quad \text{.....(1b)}$$

where (x_1, y_1) and (x_4, y_4) are the coordinates of nodes "1" and "4", respectively. If the coordinates are updated by the corresponding displacement components, the instantaneous crack orientation can be determined. The effective length (Δa) is

$$\Delta a = \frac{1}{2}\sqrt{\left(x_4 - x_3\right)^2 + \left(y_4 - y_3\right)^2} \quad \ldots.. (2)$$

where (x_3, y_3) are the coordinates of node "3".

When the DCZM element is placed at the crack tip between nodes "1" and "2", the strain energy stored is

$$\begin{aligned} &\mathrm{E} = \frac{1}{2}K_{\overline{X}}\left[X_1\right]^2 + \frac{1}{2}K_{\overline{Y}}\left[Y_1\right]^2, \\ &X_1 = (U_1\cos\theta + U_2\sin\theta) - (U_3\cos\theta + U_4\sin\theta), \\ &Y_1 = (-U_1\sin\theta + U_2\cos\theta) - (-U_3\sin\theta + U_4\cos\theta) \end{aligned} \qquad (3)$$

where, $K_{\overline{X}}$ and $K_{\overline{Y}}$ are values of the stiffness in the local coordinate system ($\overline{X}, \overline{Y}$), see Figure 2. They act to sense crack sliding and crack opening, respectively. The variation of the strain energy is, therefore,

$$\delta\mathrm{E} = \delta\mathbf{U}^T \begin{bmatrix} \mathrm{K}_s & -\mathrm{K}_s \\ -\mathrm{K}_s & \mathrm{K}_s \end{bmatrix} \mathbf{U} = \delta\mathbf{U}^T \mathrm{K}\mathbf{U} \qquad (4)$$

where

$$\mathrm{K}_s = \begin{bmatrix} \cos\theta & -\sin\theta \\ \sin\theta & \cos\theta \end{bmatrix} \begin{bmatrix} K_{\overline{X}} & 0 \\ 0 & K_{\overline{Y}} \end{bmatrix} \begin{bmatrix} \cos\theta & \sin\theta \\ -\sin\theta & \cos\theta \end{bmatrix} = \mathbf{T}^T \overline{\mathrm{K}}_s \mathbf{T} \qquad (5a)$$

$$\mathbf{U} = \begin{Bmatrix} U_1 \\ U_2 \\ U_3 \\ U_4 \end{Bmatrix}; \quad \delta\mathbf{U} = \begin{Bmatrix} \delta U_1 \\ \delta U_2 \\ \delta U_3 \\ \delta U_4 \end{Bmatrix} \qquad (5b)$$

"K" is the stiffness matrix for the element in the global coordinate system, and is required for the user defined element subroutine in ABAQUS®. "**U**" is the displacement vector related to nodes "1" and "2". The nodal opening at the crack tip is:

$$\delta = -(U_1 - U_3)\sin\theta + (U_2 - U_4)\cos\theta \qquad (6)$$

In the present study, a triangular cohesive law ([23], [47-49]) is used as shown in Figure 3. Based on the energy required to create a new crack surface, we have,

$$\frac{1}{2}\sigma_c\delta_m = G_{IC} \quad (7)$$

where G_{IC} is the fracture toughness of the material that can be measured through tests. δ_m, and σ_c are the maximum nodal opening and the critical cohesive stress, respectively. Once one of them is chosen, the other is determined by equation (7) and thus the cohesive law is completely fixed. In this paper, we choose δ_m as the cohesive parameter. The numerical value of δ_m is determined via trials until the variation of δ_m does not affect the fracture load significantly. Once δ_m is chosen, the critical value for the cohesive force in the DCZM element is calculated as

$$F_c = \sigma_c B\Delta a = \frac{2G_{IC}B\Delta a}{\delta_m} \quad (8)$$

where, B is the out-of-plane thickness of the specimen. Since the spacing of the DCZM element depends on the coordinates of the nodes, F_c depends on the mesh size (note σ_c is independent of element spacing). The critical opening (δ_c) is calculated by

$$\delta_c = \frac{F_c}{K_{\bar{y}}} \quad (9)$$

where $K_{\bar{Y}}$ is the initial stiffness of the DCZM element which is selected to be a very high value relative to the stiffness of the bridged material.

To apply the triangular cohesive law, when $\delta \le \delta_c$, $K_{\bar{Y}}$ is set to be a very large number to ensure that the crack is initially closed. In numerical implementation, this value usually is chosen to be three orders of magnitude larger than the major Young's modulus of the specimen. When $\delta_c < \delta < \delta_m$, the softening part of the cohesive zone, $K_{\bar{Y}}$ is determined as

$$K_{\bar{Y}} = -\frac{F_c}{\delta_m - \delta_c} \quad (10)$$

Finally, when $\delta \ge \delta_m$, the DCZM element fails completely, and $K_{\bar{Y}} = 0$.

For mixed mode failure, the DCZM implementation is as illustrated in Figure 4. Two one-dimensional cohesive elements are placed along the intended crack path. Both elements are attached to the same two nodes on the crack flanges. Once the following criterion is satisfied,

$$\frac{G_I}{G_{IC}} + \frac{G_{II}}{G_{IIC}} \ge 1 \quad (11)$$

both 1D elements are completely removed, and the crack is assumed to have advanced to that location. Note that the DCZM implementation is not tied to the form of the "failure criterion". Equation (11) is chosen in the present study based on past experience and success in using this for failure prediction [54].

Application of DCZM to predict mode I fracture of 2DTBC

Figure 5 shows a schematic of the SENB test set-up. The front surface of the specimen is lightly coated with a diffusely reflective white surface to improve image quality. This surface is illuminated with a He-Ne laser. During crack growth, extensive fiber bridging is clearly observed, see inset of Figure 5. Further details of the experiments and the experimental data are given elsewhere [22, 55]. Figure 6 presents the test results for mode I fracture toughness (G_{IC}) measured using the compliance method. It is seen that the fracture toughness varies with respect to the crack extension during the initial stages of crack growth and then attains an approximately constant plateau value. It is noted that, the G_{IC} value that is measured in the experiments is a through the thickness averaged fracture energy. The position of the crack path (with respect to the braid microstructure and with respect to the details of the stacking) varies from specimen to specimen. It is not unusual to find variation in the G_{IC} values (for the through the thickness averaged) in this class of composites. On the other hand for a single layer of the textile composite and for a crack path position that is consistent with respect to the textile architecture, the G_{IC} value can be obtained more consistently and with less scatter.

Due to symmetry, only one half of the fracture specimen is modeled with FEA, as shown in Figure 7. Three different meshes corresponding to different numbers of elements (1610, 6570 and 26280 elements, respectively), are used to study the mesh sensitivity of the DCZM [55]. The specimen is modeled with CPS4 elements in ABAQUS with mechanical properties listed in Table 1. The load application roller and the support rollers are modeled by CPS3 elements with mechanical properties of steel. Contact surfaces are applied between the rollers and the specimen.

The load is applied in the form of displacement control (Δ) at the center of the loading roller. The force (P) is taken as the contact force between loading roller and the upper surface of the specimen and, therefore, it is comparable to the force measured from the load cell in experiments.

The mechanical characterization of the 2DTBC is reported in [55]. It is found that the 2DTBC can be modeled as a orthotropic elastic plastic solid with a one parameter plastic potential [55], with the "a_{66}" parameter = 1.2. A user defined material subroutine UMAT is used to accommodate the orthotropic plastic model. This is done in conjunction with the user element subroutine for the DCZM. The P vs. Δ curves for this case is shown in Figure 8. Mesh (b) and mesh (c) prediction are very close to each other, and the difference between the two can be neglected. It is clear that the DCZM results have converged with respect to mesh size. In general, the simulated results by DCZM agree very well with the test data. In using the present DCZM, no numerical convergence problems are encountered. The method did not show any significant mesh sensitivity. Table 2 summarizes the CPU times used for the simulations. Each analysis job is run on a SunBlade 100 machine with one processor (UNIX environment). For the mesh with the least number of elements without plasticity, the CPU consumed for a complete analysis is approximately ten minutes. This is a great reduction in time compared to similar runs with CCZM which can take CPU times on the order of hours.

Application of DCZM to predict mixed mode fracture of MMB

The MMB set-up was introduced by Reeder and Crews [57] to obtain mixed-mode fracture data using a relatively simple test machine and test fixture. The configuration used in the MMB is shown in Figure 9. An edge cracked unidirectional composite beam is subjected to load as shown. The edge crack 'splits" the beam of thickness 2h into two beams of thickness h. By changing the load application point, a variety of mixed-mode conditions can be implemented. An analytical solution for the P vs. Δ relation corresponding to Figure 9 is formulated in [25]. In order to compare the DCZM solution with the analytical solution in [25], the following geometrical dimensions and material properties are used in the analysis;

L=50mm; e=50mm; a_0=30mm; h=1.5mm;
B=10.0mm, $E=135\times10^3$MPa; v=0.24; $G_{IC}=G_{IIC}$=4.0N/mm

Figure 10 shows a comparison of results between the analytical solution and the FEA results using the DCZM for different pairs of cohesive strength (σ_{1c}, σ_{2c}). As the mode I and mode II cohesive strengths increase, the present DCZM results approach the analytical results. The analytical results are based only on LEFM and has no "strength" information in assessing failure. On the other hand, the DCZM incorporates both, a critical strength and a critical energy release rate, in assessing failure. No convergence problems are encountered in the implementation. This indicates that the implementation of the mixed-mode DCZM, as proposed herein, is indeed satisfactory for this class of problems.

Conclusions

In this paper, results from a novel discrete cohesive zone model (DCZM) to simulate mode I and mixed mode fracture have been presented. For the mode I case, experimental results generated using a modified single edge notched bend specimen of a 2D triaxially braided composite (2DTBC) are used to verify the DCZM. The mixed mode bending (MMB) fracture test configuration developed by Reeder and Crews [57] is used as the configuration to study mixed mode fracture. In both cases, it is seen that the DCZM is able to capture the essential features of the fracture problems. The DCZM, as presented here, is easy to implement and is computationally efficient when compared to other cohesive zone modeling approaches. Because the DCZM uses a "point-wise" discrete approach to simulate fracture and because the FEA is essentially a discrete solver, the two approaches are compatible and this is reflected in the computational expediency in the numerical implementation of the DCZM.

Acknowledgements

The authors wish to thank the DOE program management team and the Board and staff of the Automotive Composites Consortium-Energy Management Working Group. This work was sponsored by the Automotive Composites Consortium and the US Department of Energy, Office of Transportation Technologies, Office of Advanced Automotive Technologies, Lightweight Materials Program under Cooperative Agreement number FC05-02OR22910). DX, AGS and AMW wish to thank the Aerospace Engineering Department at the University of Michigan.

References

1. Chou TW, Microstructural Design of Fiber Composites, Cambridge University Press, Cambridge, 1992.
2. Poe CC, Dexter HB and Raju IS, Review of the NASA textile composites research, Journal of Aircraft, 36 (1999): 876-884.
3. Ramani K and Dai HM, Design and process for preformed woven, knitted, and braided thermoplastic composite reinforced arrester, Journal of Composite Materials, 36(2002): 2357-2372.
4. Huang ZM, Modeling and characterization of bending strength of braided fabric reinforced laminates, Journal of Composite Materials, 36(2002): 2537-2566.
5. Huang ZM and Ramakrishna S, Modeling inelastic and strength properties of textile laminates: a unified approach, Composites Sciences and Technology, 63(2003): 445-466.
6. Byun JH, The analytical characterization of 2-D braided textile composites, Composites Science and Technology, 60(2000): 705-716.
7. Tang XD and Whitcomb JD, Progressive failure behaviors of 2D woven Composites, Journal of Composite Materials, 37(2003): 1239-1259.
8. Quek SC, Waas AM, Shahwan KW and Agaram V, Analysis of 2D triaxial flat braided textile composites, International Journal of Mechanical Sciences, 45(2003): 1077-1096.
9. Song SJ and Waas AM, Response and stability of woven composites under compressive loads, ICCES'04, Portugal, July 2004.
10. Glaessgen EH, Pastore CM, Griffin OH and Birger A, Geometrical and finite element modeling of textile composites, Composites: Part B, 27(1996): 43-50.
11. Quek SC, Waas AM, Shahwan KW and Agaram V, Compressive response and failure of braided textile composites: Part 1- experiments, International Journal of Non-linear Mechanics, 39(2004): 635-648.
12. Quek SC, Waas AM, Shahwan KW and Agaram V, Compressive response and failure of braided textile composites: Part 2- computations, International Journal of Non-linear Mechanics, 39(2004): 649-663.
13. Noh JH and Whitcomb JD, Progressive damage simulation of thick viscoelastic laminate with homogenization technique, Mechanics of Advanced Materials and Structures, 10 (2003): 285-302.
14. Woo K and Whitcomb JD, Three-dimensional failure analysis of plain weave textile Composites using a global/local finite element method, Journal of Composite Materials,30 (1996): 984-1003.
15. Quek SC, Waas AM, Hoffman J and Agaram V, The crushing response of braided and CSM glass reinforced composite tubes, Composite Structures, 52(2001): 103-112.
16. Rybicki EF and Kanninen MF, Finite-element calculation of stress intensity factors by a modified crack closure integral, Engineering Fracture Mechanics, 9 (1977): 931-938.
17. Kutlu Z and Chang FK. Modeling compressive failure of laminated composites containing multiple through-the-width cracks. Journal of Composite Materials, 26(1992): 350-387.
18. Tsai JL, Guo C and Sun CT. Dynamic crack fracture toughness in unidirectional polymeric composites. Composites Science and Technology, 61(2001): 87-94.
19. Xie D and Biggers, Jr. SB, Progressive crack growth analysis using interface element based on the virtual crack closure technique, Finite Elements in Analysis and Design, in preparation.
20. Xie D, Waas AM, Shahwan KW, Schroeder JA and Boeman RG, Computation of energy release rates for kinking cracks based on virtual crack closure technique, CMES: Computer Modeling in Engineering & Sciences, 6(2004): 515-524.

21. Salvi AG, Chung J, Waas AM and Caliskan A, Strain-rate effects on unidirectional carbon-fiber composites, AIAA Journal, 41 (2003): 2020-2028.
22. Salvi AG, Waas AM and Caliskan A, Static and dynamic fracture of 2DTBC, in preparation for publication.
23. Ungsuwarungsri T and Knauss WG, The Role of Damage-Softened Material Behavior in the fracture of composites and adhesives, International Journal of Fracture, 35(1987): 221-241. See also Ph.D. thesis, 1985, Aeronautics Department, Caltech, Pasadena, CA.
24. Xu XP and Needleman A, Numerical simulation of fast crack growth in brittle solids, Journal of the Mechanics and Physics of Solids, 42(1994): 1397-1434.
25. Mi Y, Crisfield MA, Davis GAO and Helweg HB, Progressive delamination using interface elements, Journal of Composites, 32(1998): 1246-1272.
26. de Borst R, Numerical aspect of cohesive zone models, Engineering Fracture Mechanics, 70(2003): 1943-1961.
27. Yang QD and Thouless MD, Mixed-mode fracture analyses of plastically-deforming adhesive joints, International Journal of Fracture, 110 (2001): 175-187.
28. Yang QD, Thouless MD and Ward SM, Numerical simulations of adhesively-bonded beams failing with extensive plastic deformation, Journal of the Mechanics and Physics of Solids, 47 (1999): 1337-1353.
29. Li S, Wang J and Thouless MD, The effects of shear on crack in layered materials, Journal of the Mechanics and Physics of Solids, 52(2004): 193-214.
30. Li S, Thouless MD, Waas AM, Schroeder JA and Zavattieri PD, Mode-I cohesive-zone models for fracture of an adhesively bonded polymer-matrix Composite, Composites Science and Technology, accepted to appear, 2004.
31. Li S, Thouless MD, Waas AM, Schroeder JA and Zavattieri PD, Use of cohesive-zone models to analyze fracture of a fiber-reinforced polymer-matrix Composite, Composites Science and Technology, accepted to appear, 2004.
32. Zavattieri PD, Raghuram PV and Espinosa HD, A computational model of ceramic microstructures subjected to multi-axial dynamic loading, Journal of the Mechanics and Physics of Solids, 49 (2001): 27-68.
33. Espinosa HD, Zavattieri PD and Dwivedi SK, A finite deformation continuum discrete model for the description of fragmentation and damage in brittle materials, Journal of the Mechanics and Physics of Solids, 46 (1998): 1909-1942.
34. de Moura MFSF, Goncalves JPM, Marques AT and de Castro PMST, Prediction of compressive strength of carbon-epoxy laminates containing crack by using a mixed-mode damage model, Composite Structures, 50(2000): 1415-1438.
35. Camacho GT and Ortiz M, Computational modeling of impact demage in brittle materials, International Journal of Solids and Structures, 33(1996): 2899-2938.
36. Zou Z, Reid SR and Li S, A continuum damage model for delaminations in lamianted Composites, Journal of the Mechanics and Physics of Solids, 51(2003): 333-356.
37. Zhou F and Molinari JF, Dynamic crack propagation with cohesive elements: a methodology to address mesh dependency, International Journal for Numerical Methods in Engineering, 59(2004): 1-24.
38. El-Sayed S and Sridharan S, Cohesive models for predicting delamination growth and crack kinking in sandwich structures, International Journal of Fracture, 117(2002): 63-84.
39. Reedy ED, Mello FJ and Guess TR, Modeling the initiation and growth of delaminations in composite structures, Journal of Composite Materials, 31 (1997): 812-831.

40. Tvergaard V and Hutchinson JW, The relation between crack growth resistance and fracture parameters in elastic-plastic solids, Journal of the Mechanics and Physics of Solids, 40(1992): 1377-1397.
41. Goyal V and Klug J, Interphasic formulation for the prediction of delamination, AIAA-2004-1845, 45th AIAA/ASME/ASCE/AHS/ASC Structures, Structural Dynamics and Materials conference, Palm Spring, Ca, April 19-22, 2004.
42. Goyal V and Johnson E, Cohesive-Decohesive interfacial constitutive law for the analyses of fatigue crack initiation and growth, AIAA-2004-1678, 44th AIAA/ASME/ASCE/AHS/ASC Structures, Structural Dynamics and Materials conference, Norfolk, Virginia, April 7-10, 2003.
43. Goyal-Singhal V, Jaunky N, Johnson E and Ambur D, Intralaminar and interlaminar progressive failure analyses of composite panels with circular cutouts, AIAA-2004-1745, 43rd AIAA/ASME/ASCE/AHS/ASC Structures, Structural Dynamics and Materials conference, Denver, Colorado, April 22-25, 2002.
44. de Borst R, Some recent issues in computational failure mechanics, International Journal for Numerical Methods in Engineering, 52(2001): 63-95.
45. de Borst R, Numerical aspects of cohesive-zone models, Engineering Fracture Mechanics, (2003).
46. Schellekens J C J and de Borst R, On the numerical integration of interface elements, International Journal for Numerical Methods in Engineering, 36(1993): 43-66.
47. Song SJ and Waas AM, Energy-based mechanical model for mixed-mode failure of laminated composites, AIAA Journal, 33 (1995): 739-745
48. Song SJ and Waas AM, Mode-I failure of laminated polymeric composites, Engineering Fracture Mechanics, 49 (1994): 17-27.
49. Song SJ and Waas AM, A spring foundation model for mode-I failure of laminated composites based on an energy criterion, Journal of Engineering Materials and Technology, 116 (1994): 512-516.
50. Shahwan KW and Waas AM, Non-self-similar decohesion along a finite interface of unilaterally constrained delaminations, Proceedings of the Royal Society of London. Series A: Mathematical and Physical Sciences, 453 (1997): 515-550.
51. Sun C, Waas AM, Li S, Thousless MD, Schroder JA and Zavattieri PD, Out-of-plane fracture characterization of a composite using discrete cohesive zone model: experiments and analysis, in preparation.
52. Pietruszczak S and Mroz Z, Finite element analysis of deformation of strain softening materials, International Journal for Numerical Methods in Engineering, 17 (1981): 327-334.
53. ABAQUS Inc., ABAQUS User Manual, version 6.3, Pawtucket, RI.
54. Xie D, Waas AM, Shahwan KW, Boeman RG and Schroeder JA, Fracture criteria for kinking cracks in triple material bonded joints, Engineering Fracture Mechanics, accepted.
55. Xie D, Salvi AG, Waas AM, Caliskan A, Discrete cohesive zone model to study static fracture in a plate of textile braided carbon fiber composites, International Journal for Numerical Methods in Engineering, submitted.
56. Sun CT and Chen JL, A plastic potential function suitable for anisotropic fiber composites, Journal of Composite Materials, 27(1993): 1379-1390.
57. Reeder JR and Crews JR, Mixed-mode bending for delamination testing, AIAA Journal, 28(1990):1270-1276.

Table 1. Effective Mechanical Properties

E_{11}(GPa)	E_{22}(GPa)	ν_{12}	G_{12}(GPa)
68.53	10.78	0.36	4.52

Table 2. CPU consumed by DCZM (unit: second)*

Conditions	Mesh (a) 1610 elements	Mesh(b) 6570 elements	Mesh (c) 26280 elements
G_{IC}=57N/mm, No a_{66}	506	2236	10277
G_{IC}=f(Δa), No a_{66}	499	2243	10103
G_{IC}=f(Δa) and a_{66}	1227	6446	31927

*SunBlade 100 machine, UNIX

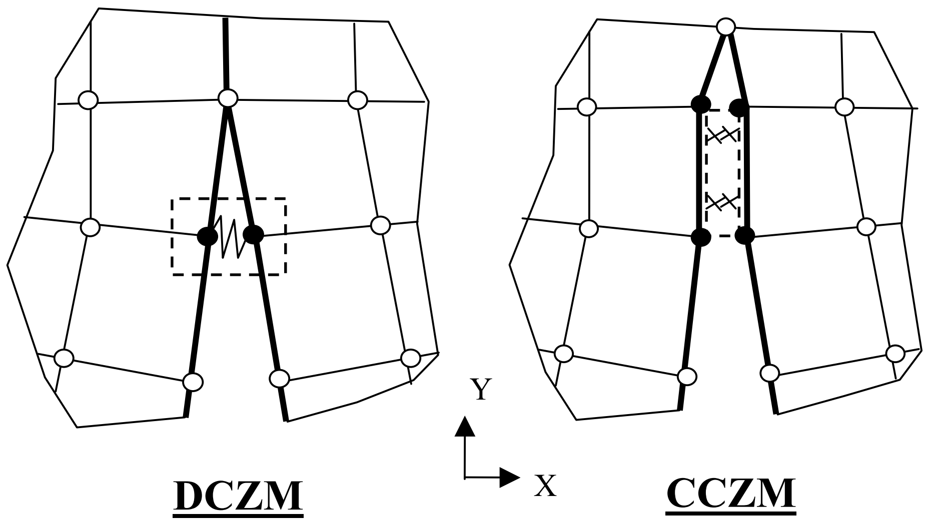

Figure 1: Scheme of DCZM and CCZM

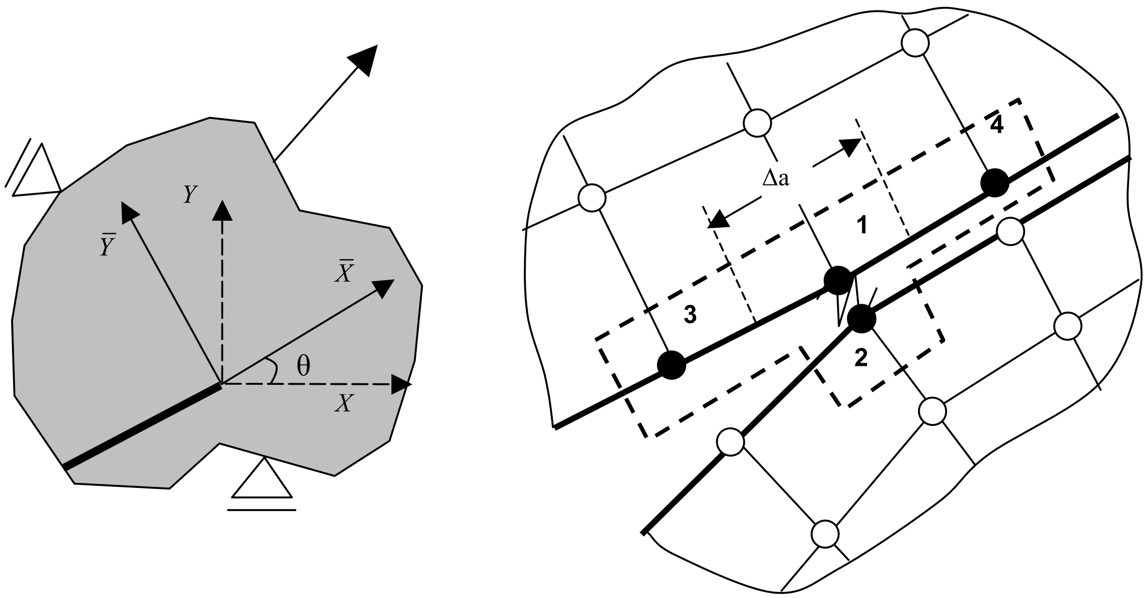

Figure 2: DCZM interface elements for slant crack lying in (X, Y) plane

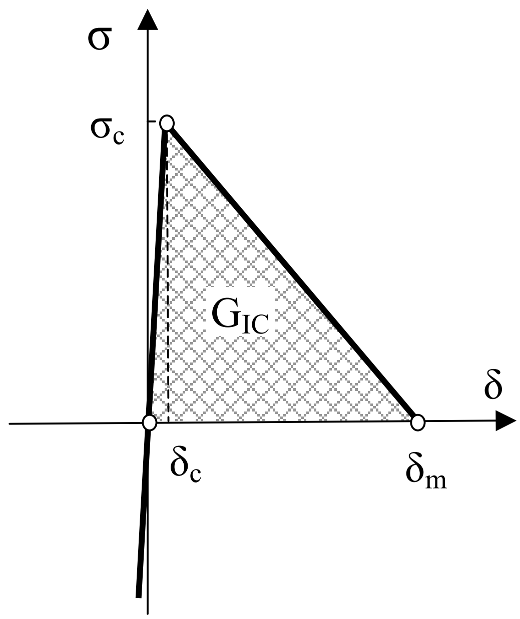

Figure 3: Triangle type cohesive law used in the present study

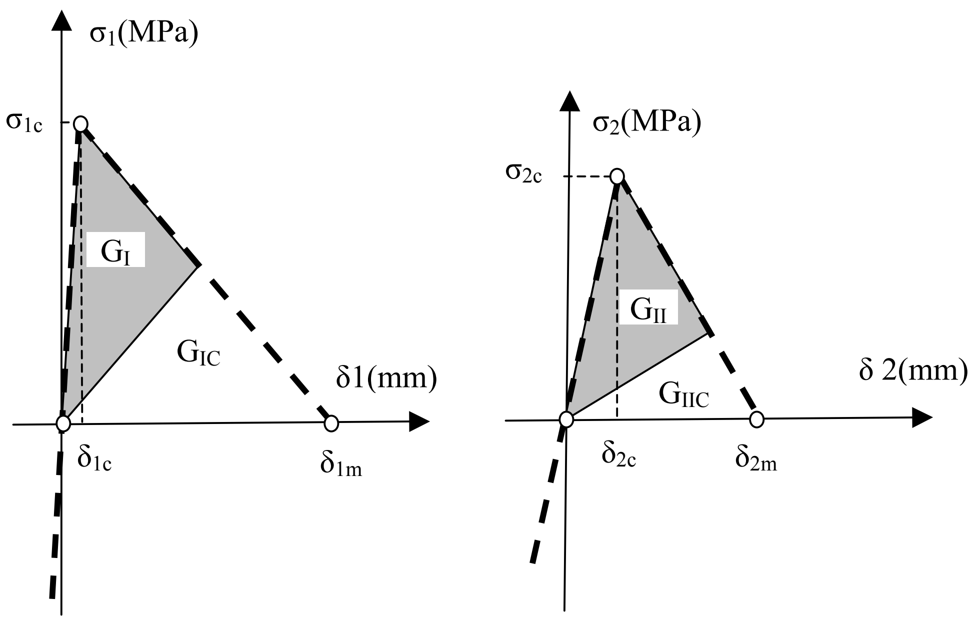

Figure 4: Fracture criterions for mixed mode fracture in DCZM

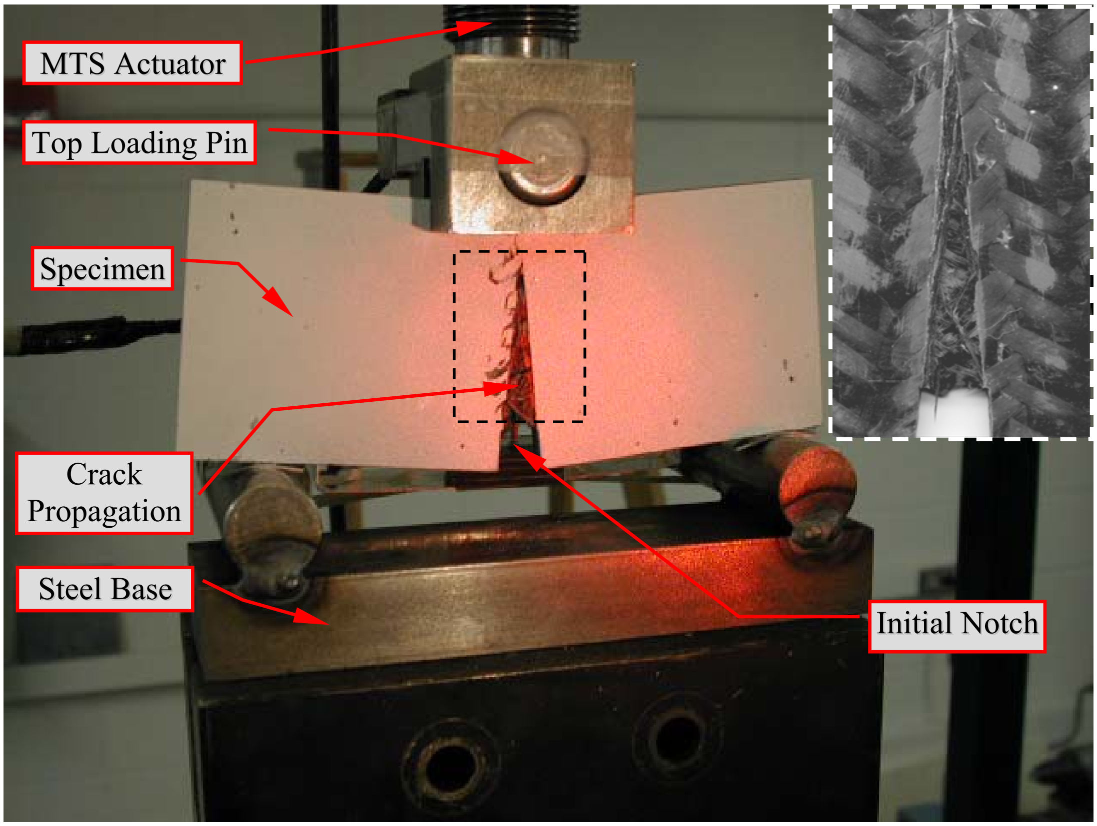

Figure 5: Experimental setup for fracture toughness tests.

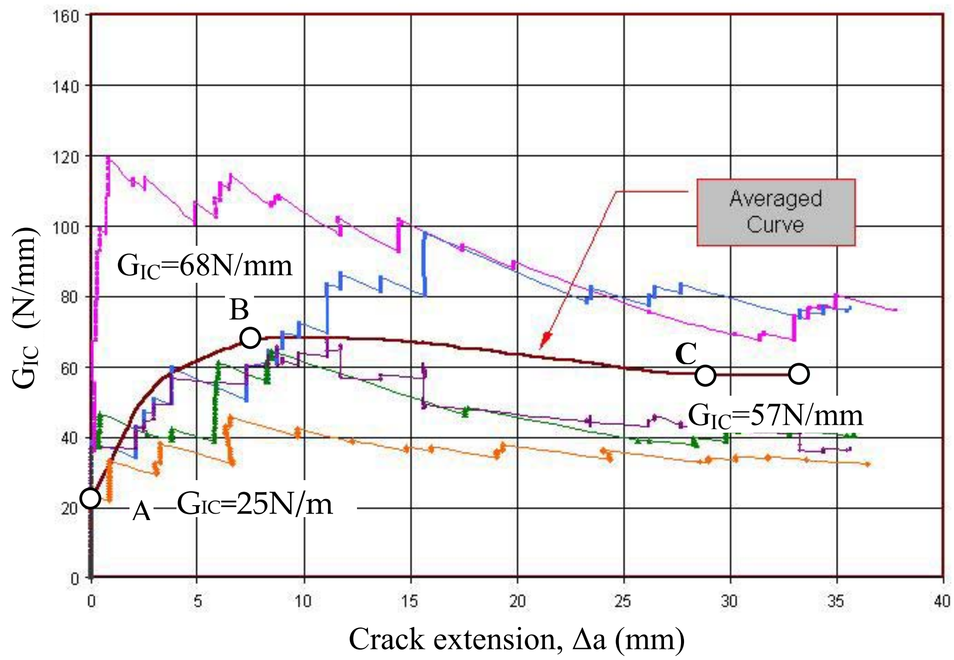

Figure 6: Fracture toughness varied with crack extension averaged from test data

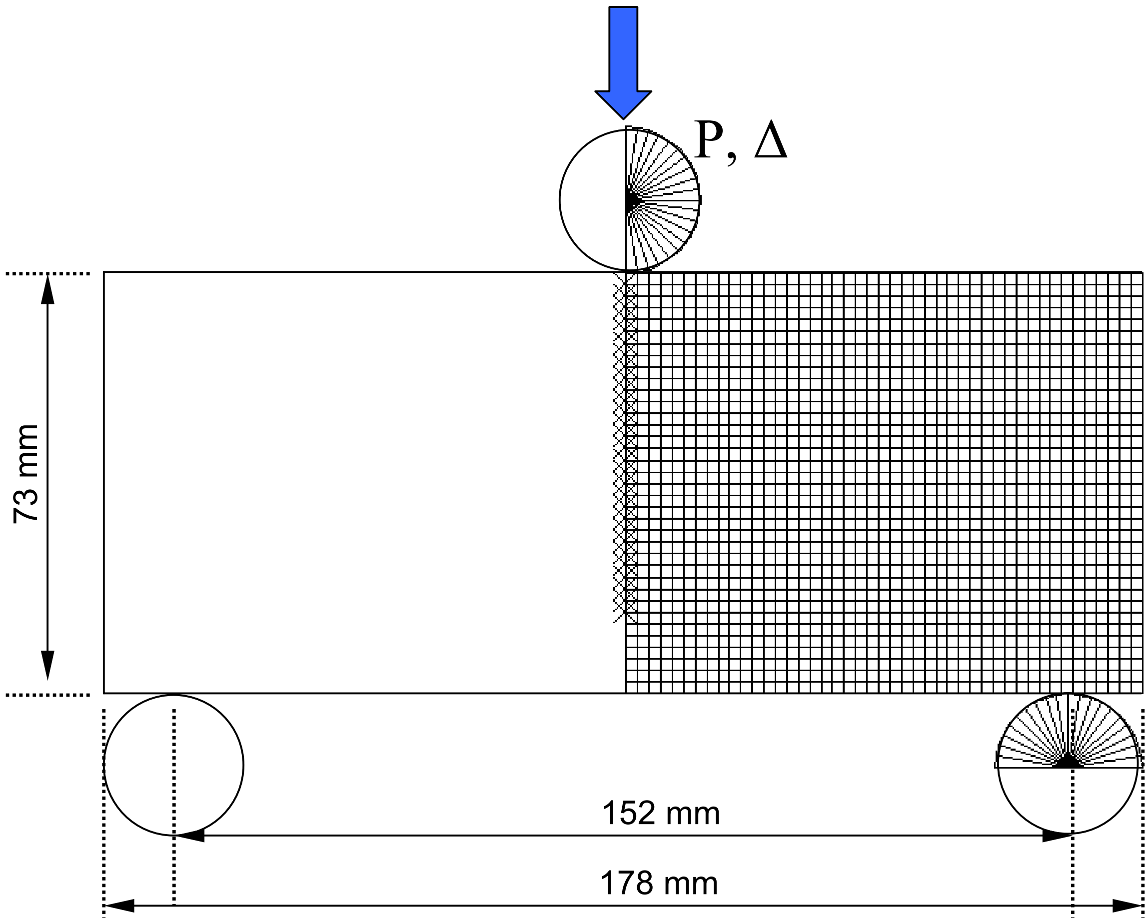

Figure 7: Single edge notch bend specimen to measure fracture toughness1610 elements

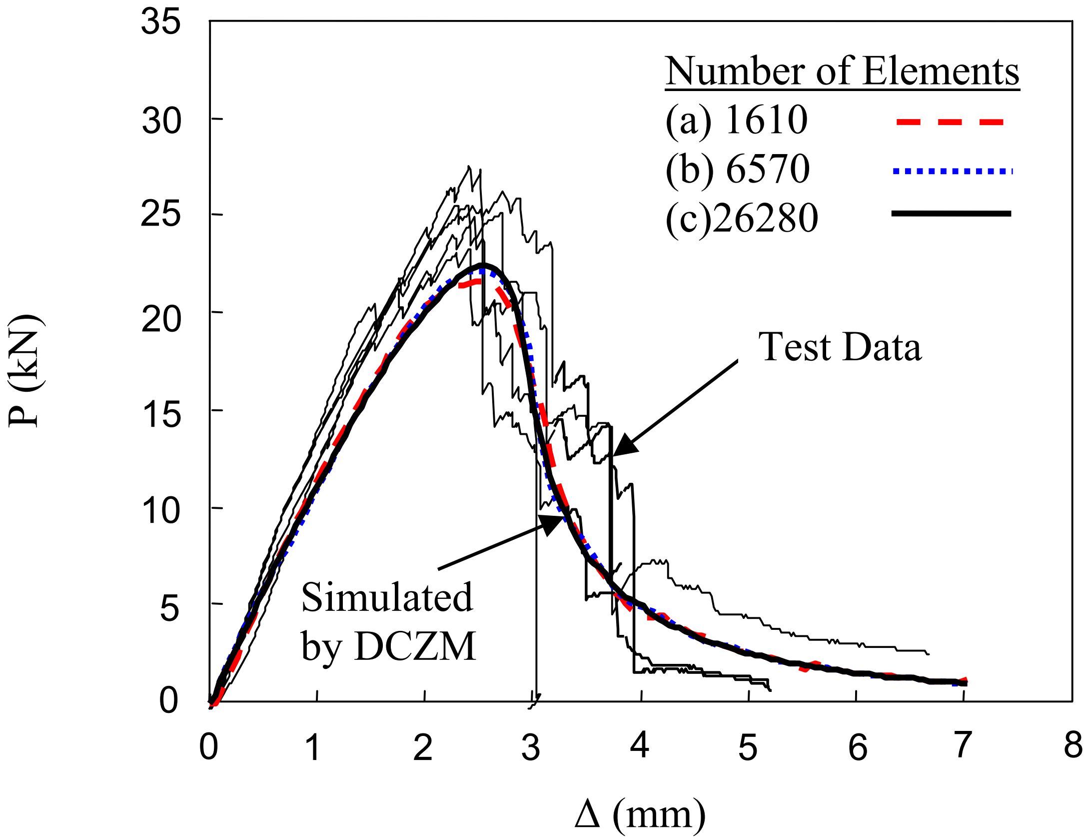

Figure 8: Comparison between test data and simulated results by DCZM (G_{IC}=f(Δa) and a_{66})

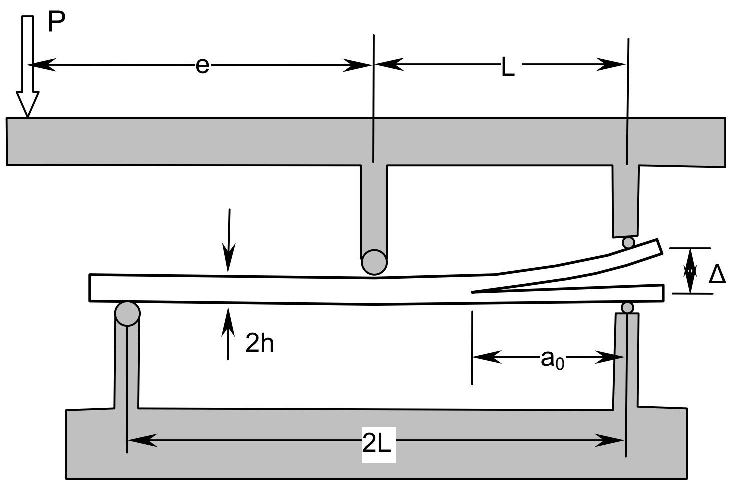

Figure 9: Mixed-Mode Bending (MMB) Test Apparatus

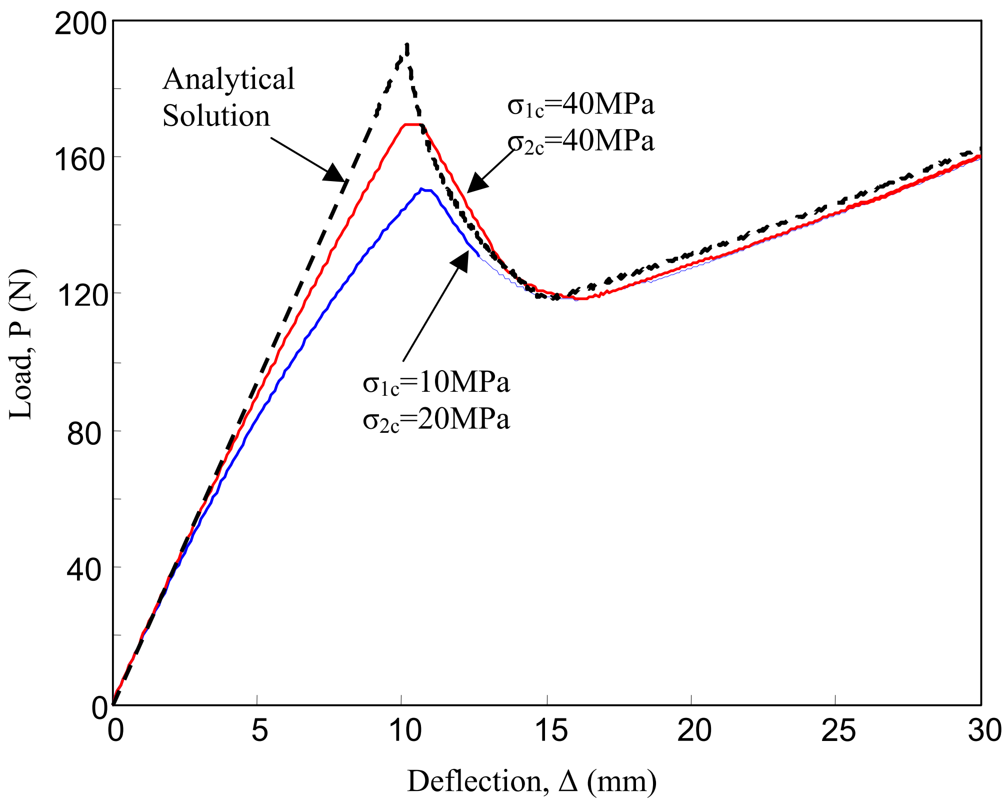

Figure 10: Comparison of analytical solution and DCZM for MMB